White Rose Research Online

eprints@whiterose.ac.uk
https://eprints.whiterose.ac.uk
Universities of Leeds, Sheffield and York

Deposited via The University of Leeds.

White Rose Research Online URL for this paper:
https://eprints.whiterose.ac.uk/id/eprint/215628/

Version: Accepted Version

Proceedings Paper:
Lang, A.J., Connolly, D.P., de Boer, G. et al. (2024) Confined Transonic Aerodynamics: From Rifle Bullets to Hyperloop Vehicles. In: AIAA Journal. AIAA Aviation Forum and ASCEND 2024, 29 Jul - 02 Aug 2024, Las Vegas, USA. American Institute of Aeronautics and Astronautics. ISSN: 0001-1452. EISSN: 1533-385X.

https://doi.org/10.2514/6.2024-3770

© 2024 by Alex J. Lang, David P. Connolly, Gregory de Boer, Benjamin Hinchliffe, Carl A. Gilkeson, Shahrokh Shahpar. This is an author produced version of a conference paper accepted for publication in AIAA Journal. Uploaded in accordance with the publisher's self-archiving policy.

Reuse
Items deposited in White Rose Research Online are protected by copyright, with all rights reserved unless indicated otherwise. They may be downloaded and/or printed for private study, or other acts as permitted by national copyright laws. The publisher or other rights holders may allow further reproduction and re-use of the full text version. This is indicated by the licence information on the White Rose Research Online record for the item.

Takedown
If you consider content in White Rose Research Online to be in breach of UK law, please notify us by emailing eprints@whiterose.ac.uk including the URL of the record and the reason for the withdrawal request.

UNIVERSITY OF LEEDS
University of Sheffield
UNIVERSITY of York

AIAA Aviation Forum and ASCEND co-located Conference Proceedings
29 July - 2 August 2024, Las Vegas, Nevada
AIAA AVIATION FORUM AND ASCEND 2024
10.2514/6.2024-3770

Confined Transonic Aerodynamics: From Rifle Bullets to Hyperloop Vehicles

Alex J. Lang[1], David P. Connolly[2], Gregory de Boer[3], Benjamin Hinchliffe[4], and Carl A. Gilkeson[5]
University of Leeds, Leeds, West Yorkshire, LS2 9JT, United Kingdom

Shahrokh Shahpar[6]
Imperial College, London, SW7 2AZ, United Kingdom

Downloaded by Carl Gilkeson on July 30, 2024 | http://arc.aiaa.org | DOI: 10.2514/6.2024-3770

The Hyperloop concept, which uses partially evacuated tubes to transport passenger pods at high speeds, has attracted significant attention in recent years as a potential future mode of travel. Hyperloop presents a unique aerodynamics problem as it sits at the intersection of transonic, low Reynolds number and confined/choked flow. Consequently, very little experimental research has been conducted on the aerodynamics of Hyperloop-type systems, making validation of simulation methods very difficult. Here, we draw attention to a preexisting experimental data set for a transonic bullet, travelling at Mach 1.1 in ground-effect. This is the basis for validating Computational Fluid Dynamics (CFD) simulations and these are shown to accurately replicate pressure distributions. Next, the computational approach is extended, culminating in aerodynamic simulations of a generic Hyperloop system. This is achieved by successively making the following changes to the validated projectile model, while keeping all other variables and settings consistent: (i) scale, (ii) operating pressure, (iii) full-tube confinement, and (iv) tail geometry. Flow choking is found to dominate the flow characteristics within the tube, however, extremely low aerodynamic drag levels are predicted, underlining the clear potential of the fundamental concept. It is envisaged that the generic Hyperloop pod design presented here will form the basis for a benchmark case to assist wider research efforts in this area.

I. Introduction

In 2013 Elon Musk and SpaceX proposed the idea of transporting passengers in pods through an underground network of tubes operating at very low pressure [1]. The purpose of the low-pressure environment (on the order of 0.1% of atmospheric pressure) is to dramatically reduce aerodynamic drag such that operational speeds in the transonic regime can be realized. This concept is known as Hyperloop [1] and it is essentially a form of ultra-high-speed rail. Whilst Hyperloop may seem to be relatively new, the notion of evacuated tube transport has received attention for many years under various guises. In fact, its origins date back to the 18th century when pneumatic tube system designs were pioneered by both George Medhurst and William Murdoch. The purpose was to transport goods more efficiently by generating a partial vacuum [2, 3]. Later, Isambard Kingdom Brunel was involved in the development of so-called atmospheric railways which utilized differential air pressure to provide propulsion. For a period, these were viewed

[1] Ph.D student, EPSRC CDT in Fluid Dynamics, School of Computing.
[2] Professor, Institute for High Speed Rail and System Integration, School of Civil Engineering.
[3] Associate Professor, Institute of Thermofluids, School of Mechanical Engineering.
[4] Aeronautical and Aerospace Industrial Advisory Board Member, School of Mechanical Engineering.
[5] Lecturer, Institute of Thermofluids, School of Mechanical Engineering, corresponding author: C.A.Gilkeson@leeds.ac.uk
[6] Visiting Professor, Department of Aeronautics, AIAA Fellow.

Copyright © 2024 by Alex J. Lang, David P. Connolly, Gregory de Boer, Benjamin Hinchliffe, Carl A. Gilkeson, Shahrokh Shahpar. Published by the American Institute of Aeronautics and Astronautics, Inc., with permission.

as a viable alternative to traditional steam trains, but operational challenges ultimately led to the idea being abandoned [4].

The first known discussion of what is now recognized as Hyperloop was suggested by pioneering rocket engineer Robert Goddard in 1909 [5]. His vision was for a future ultra-high-speed rail system, requiring trains to be magnetically levitated to assist efficient propulsion through evacuated tubes. His work was speculative though and it was forgotten for many decades. In the 1970/80s evacuated tube transport was revived [6, 7] before the EPFL Swissmetro project, an intercity subway system, was proposed [8]. The premise of this was to employ a fully underground vacuum to connect major cities within Switzerland at speeds of up to 500 km/h. However, the small amount of aerodynamics research published on this concept [9] has limited scope and Swissmetro has not progressed beyond preliminary investigation [10, 11].

More recently, the white paper produced by Musk [1] has instigated a tremendous amount of research effort on many aspects of Hyperloop, including propulsion, levitation, energy consumption and aerodynamics. A recent review paper by Lang *et al*., 2024 [12] provides an in-depth commentary on recent advances in this area with a particular focus on aerodynamics. In the past decade, the majority of aerodynamic research into Hyperloop has been numerical. Detailed investigations into shock wave characteristics generated around pods and within tubes have been carried out [13]. Furthermore, transient effects [14, 15] and changes in flow states for typical transport speeds [16, 17] have been considered. Despite this breadth of aerodynamic research, there is no consensus on what a typical Hyperloop vehicle should look like and there are no known benchmark cases available to assess the accuracy of numerical approaches.

Experimentally, only one study of the aerodynamic characteristics of a Hyperloop pod, operating in a realistic environment, has been investigated [18]. This recent work was carried out by the Hyper Tube Express Research Team in Korea and published in 2023 [18]. Their work is the first known study to measure the strength of shock waves emanating from a Hyperloop pod within a transport tube operating at only 150 Pa, approximately 0.15% of atmospheric pressure. Shock waves were identified through static pressure measurements located along the transport tube as the pod traversed through it at speeds of 160-320 m/s. The pod design is basic, comprising a hemispherical nose section and a straight cylinder of diameter 0.0875 m for the main body with no tapering in the base region. The blockage ratio of the set-up was 34%. An elaborate experimental technique involved a high-pressure air compressor to launch the pod along an acceleration tube before it entered an air-diffusion tank coupled to a vacuum pump. This allowed the pod to travel along a downstream test section in low-pressure conditions, guided by a high-tension wire which passed through the center of the pod, longitudinally. Due to the complexity of the experimental method, aerodynamic measurements are limited in scope and, for example, measuring surface pressures on the pod has not yet been achieved.

To the best of the authors' knowledge, no Hyperloop-type experimental research exists in scenarios of very low ambient pressure, other than the investigation highlighted above [18]. However, a handful of studies have been conducted for projectiles operating at atmospheric pressure and in ground-effect. In the context of Hyperloop, the most notable studies are those of Doig *et al*., [19, 20]. They performed live firing experiments, wind tunnel testing, and CFD simulations to analyze the flow generated by a scaled-up Nosler 50gn S.H.O.T rifle bullet. The flow speed in their experimental case was Mach 1.1, which is within the speed regime proposed for Hyperloop. Furthermore, with a ground separation distance of half of the bullet diameter, this is also broadly similar to the clearance between a Hyperloop pod and tube walls. In their work, surface pressure measurements were made at numerous locations on the projectile and qualitative flow visualization provided further flow characterization. Although this body of work was done at atmospheric pressure, it provides a very good basis for developing accurate Hyperloop simulations. For this reason, the work of Doig *et al*., [19, 20] will be used to validate a computational approach described in this article.

The layout of this paper is as follows: section II describes the computational approach and details the validation results. Next, the approach is systematically extended to account for Hyperloop characteristics with key results provided in section III. A discussion and conclusions are then presented in sections IV and V, respectively.

II. Transonic Projectile Validation

As explained in the introduction, the work of Doig *et al*., [19, 20] has sufficient parallels to Hyperloop to be used as a basis for developing accurate numerical simulations. The measurements and data presented in these studies are extensive and rigorous, and so they were used as the starting point to build a computational Hyperloop model. This section outlines the simulation approach which is validated using the available experimental data.

Downloaded by Carl Gilkeson on July 30, 2024 | http://arc.aiaa.org | DOI: 10.2514/6.2024-3770

Downloaded by Carl Gilkeson on July 30, 2024 | http://arc.aiaa.org | DOI: 10.2514/6.2024-3770

A. Solution Domain and Boundary Conditions

Figure 1 shows important details of the solution domain and the bullet which were produced using Ansys Design Modeller [21]. The solution domain utilizes a symmetry plane on the vertical longitudinal plane of the bullet, as shown in Fig 1(a). The cross-section of the domain is based on a quarter circle which is extruded from the upstream to the downstream boundaries. The ground plane is modelled as a symmetry plane which corresponds to the symmetry method used in the wind tunnel experiments by Doig *et al*., [20]. Here, they arranged two nominally identical bullets, one above the other, with a separation distance of twice the required ground clearance. Experimental measurements were made on the top bullet only and this is the subject of the comparison in this study. The bullet has the no-slip condition applied and all remaining outer boundaries are assigned a pressure far-field type boundary condition with a free-stream Mach number of $M = 1.1$.

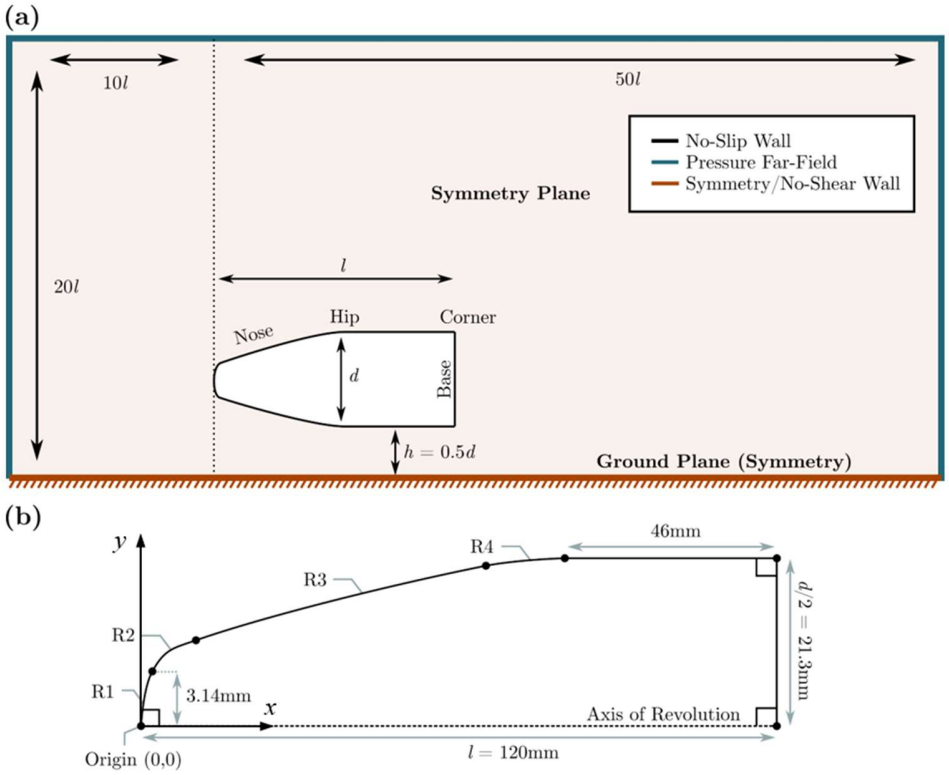

Fig. 1 Illustration of (a) solution domain and (b) geometric features of the rifle bullet for the validation case. Not to scale.

The bullet is based on a Nosler 50gn S.H.O.T projectile, which was scaled up by a factor of 7.5 to assist with instrumenting the wind tunnel model in the original experiments [20]. This exact geometry is replicated in the computational model here. Precise details of the size of the bullet are given in Fig 1(b). Note that the four radii which define the curvature of the bullet, namely, R1–R4, require individual radii center coordinates; these are presented in Table 1 and they are in relation to the origin and axis convention shown in Fig 1(b).

Table. 1 Geometrical details of radii used to define the bullet.

Symbol	Radius (mm)	Coordinate of radii center	
		x (mm)	y (mm)
R1	28.800	28.800	0.000
R2	4.500	4.645	2.649
R3	290.000	96.286	-267.743
R4	30.000	74.000	-8.700

B. Mesh Design

Poly-hexcore meshes, generated by the commercial package Ansys Fluent Meshing 2020R2 [21], were used for all simulations. This method utilizes structured hexahedral blocks in the bulk of the domain, away from the boundaries, which aligns the gridlines with the free-stream flow thereby reducing numerical diffusion. Inflation layers are used to generate structured blocks of cells around the projectile, with cell clustering at the surface to resolve the boundary layers. Polyhedral cells are then generated to fill the domain between the structured blocks. This method allows for rapid generation of meshes for complex geometries, while maintaining the benefit of being largely aligned with the free-stream flow direction. Areas of high element density were included in regions with strong expected flow gradients, such as the nose, corner and wake of the body. Adaptive refinement was also used to further increase the resolution of the mesh in the regions where shocks occur. The procedure for adaption was to equally divide cells which had the highest values for static pressure gradient. Figure 2 shows the fine mesh used in the simulations.

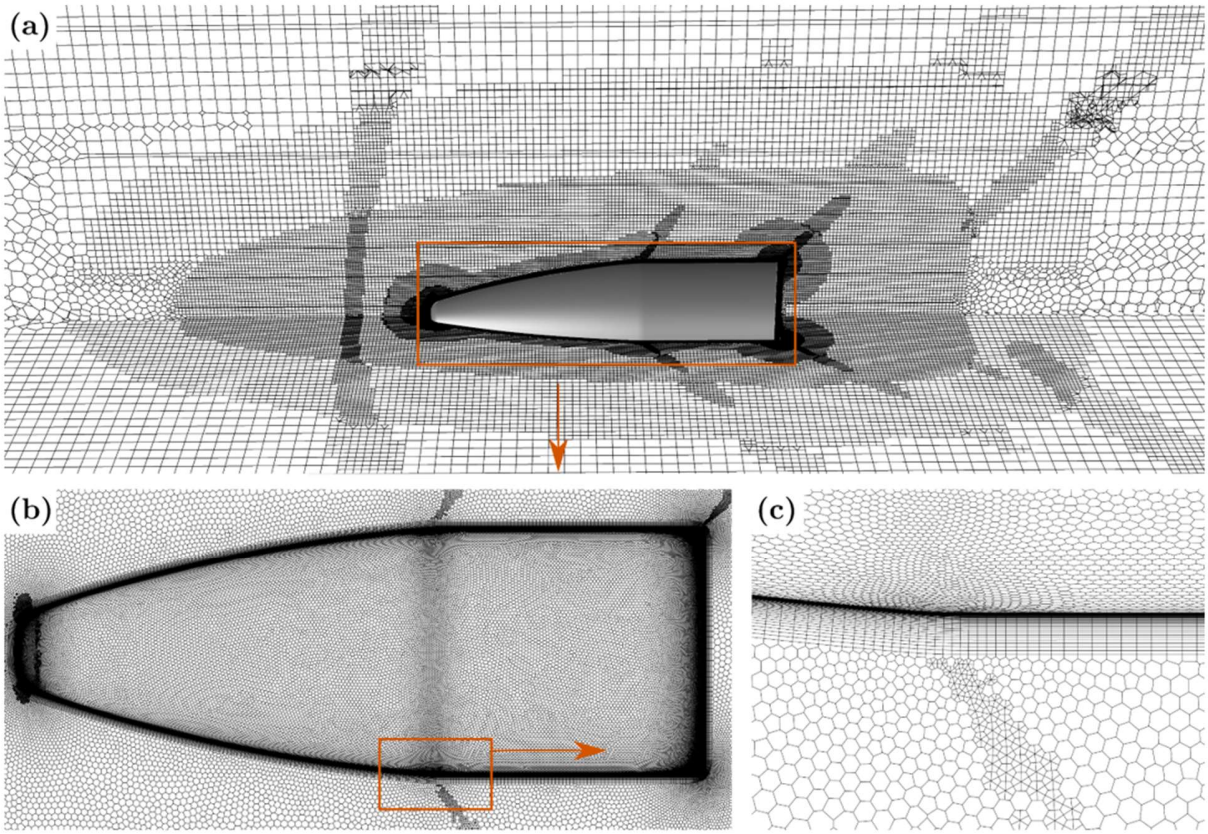

Fig. 2 Mesh structure for the validation case.

C. Solver Set-up and Mesh Independence

Three-dimensional steady-state compressible flow simulations were run using Ansys Fluent's coupled pressure-based solver [21]. Double precision real number representation was also employed to minimize round-off error. Due to the nature of the mesh structure which contains some unstructured cells to join the prismatic boundary to the hexahedral cells in the core of the domain, it was necessary to implement the least squares cell-based gradient method. Furthermore, second order discretization was employed for all equations. Taking the projectile length of 120 mm, the Reynolds number is approximately 3 million. Accordingly, the RANS-based SST k-ω turbulence model [22] was employed to assist in characterizing the flow field. This model was used with success in CFD simulations as part of the study by Doig *et al*., 2016 [20]. Each simulation was run for long enough to ensure that convergence error was eliminated. Typically, simulations would run for more than 10,000 iterations to achieve this. FMG multigrid initialization served to accelerate convergence and simulations ran in parallel on 40-core High Performance Computing (HPC) nodes with 192 GB of RAM.

Downloaded by Carl Gilkeson on July 30, 2024 | http://arc.aiaa.org | DOI: 10.2514/6.2024-3770

Investigating mesh independence involved generating four meshes each with an effective mesh refinement ratio of $r \approx 1.4$. The meshing method prescribes a constant first cell height in the definition of the prismatic boundary layer cells which envelop the bullet surfaces. The number of layers varied from 24 for the coarse mesh to 64 for the fine one. This led to a global cell count ranging from 3.65 to 17.98 million cells, see Table 2. Average wall y^+ values measured on the surface of the bullet (not including the base region where the flow is separated) were all reasonably close to the recommended value of 1. Flow simulations computed on these meshes were assessed based on the computed aerodynamic drag coefficient, C_D, as well as the lift coefficient, C_L. As shown in Table 2, the differences in the results between all solutions are small. The fine mesh design produced results which were within 1% of the extra-fine ones, thereby exhibiting low discretization errors. Accordingly, the fine mesh is used for subsequent analysis in this section.

Table. 2 Geometrical details of radii used to define the bullet.

Mesh I.D.	Cell Count	C_D	C_L	First cell height (μm)	Number of inflation layers	Wall y^+
Coarse	3,646,552	0.68487	-0.05648	3.02	24	1.26
Medium	5,393,359	0.69624	-0.05107	2.15	33	0.94
Fine	10,468,016	0.68227	-0.05449	1.54	46	0.68
Extra-fine	17,976,994	0.68020	-0.05413	1.10	64	0.51

Downloaded by Carl Gilkeson on July 30, 2024 | http://arc.aiaa.org | DOI: 10.2514/6.2024-3770

D. Validation Results

Figure 3 shows the longitudinal pressure coefficient, C_p, distribution along the length of the bullet on both the upper and lower profiles, where the bullet intersects with the longitudinal symmetry plane. Experimental data originates from the pre-existing wind tunnel tests [20] with C_p calculated at 15 pressure tap locations. These data are plotted with CFD results from [20] and those produced in the present study. Overall, the match is particularly good on the upper centerline distribution with stagnation and pressure gradients replicated very well, see Fig 3(a). A similar trend is shown for the lower centerline, Fig 3(b), although the scatter in the experimental data over the front quarter of the bullet is not reproduced. In both sets of CFD results a mild suction peak is evident in the vicinity of the nose, where the flow accelerates around the relatively small nose radius. No experimental data points exist in this precise location, but it is perfectly plausible that this particular flow feature would be present experimentally, as well.

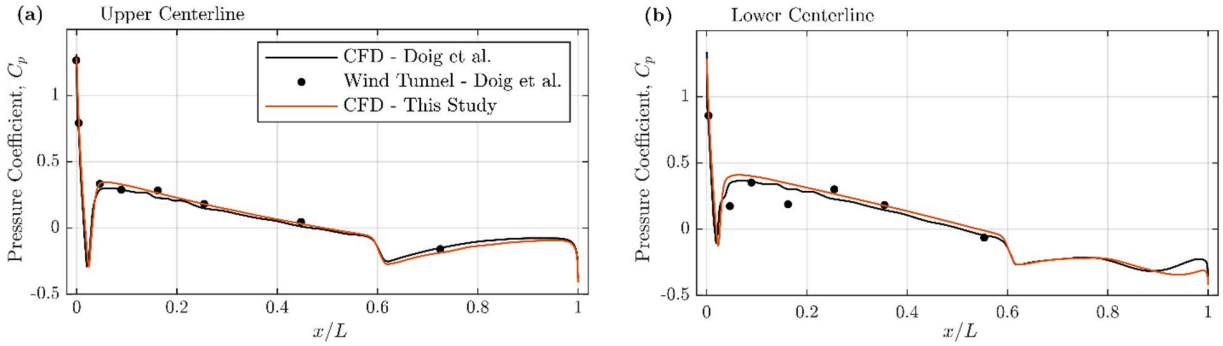

Fig. 3 Pressure coefficient distribution over (a) upper centerline and (b) lower centerline of the rifle bullet for the validation case.

Qualitatively, Fig 4 displays contours of the Mach number projected onto both symmetry planes. Due to the blunt nose geometry, a detached bow shock is generated ahead of the body. This shock bends with the flow above the projectile, however, due to the close ground-proximity, it remains normal to the flow between the nose of the bullet and the ground (symmetry) plane. Expansion waves are generated where (i) the flow turns away from the free-stream direction at the rear corner and (ii) at the mid-section where the geometry transitions to the main cylindrical portion of the bullet. On the underside of the projectile, the expansions are reflected back towards the body by the ground plane. Here, the presence of the reflecting expansions form a low pressure region, causing the wake to be deflected

downward. A recompression shock is also generated below the wake where the flow returns to approximate free-stream conditions. These flow features were observed in both wind tunnel and live firing experiments on the same projectile [23], giving confidence in the CFD results presented here.

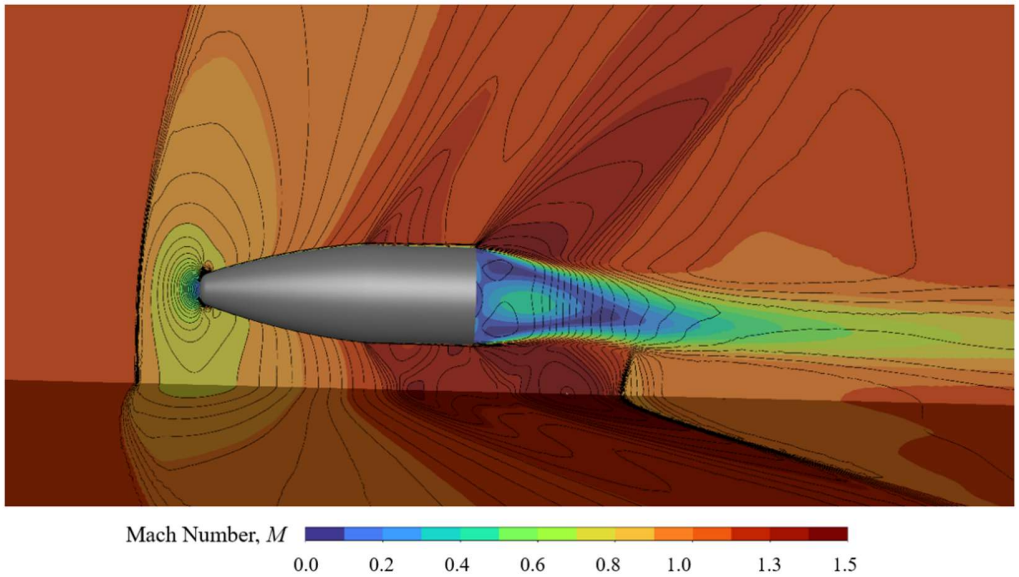

Fig. 4 Mach number contour plot projected on the two symmetry planes in the validation case.

III. Hyperloop Simulation Development

The previous section underlined the good match between experimental data and CFD simulations of a projectile in ground-effect. Similarities in projectile shape and Mach number, to those of an expected Hyperloop system, make this a sensible foundation for adding other necessary aspects. This section details the steps taken to extend the validation method such that a more realistic Hyperloop-type environment is captured.

A. Geometric Considerations and Mesh Design

In section II, the solution domain was largely unrestricted and the flow around the bullet was mainly impacted by the symmetry plane representing the ground plane. In reality, a Hyperloop system would consist of a space-limited volume surrounding each pod in the form of a transport tube. Figure 5(a) shows the projectile from the validation case placed within a tube which is twice the diameter of the projectile itself. It is important to appreciate that a Hyperloop pod would not have the blunt base geometry which is typical of projectiles, as this generates a large wake. Therefore, to create another more realistic geometry for a Hyperloop pod, the nose of the projectile geometry was reflected to produce a tapered tail which reduces the wake size. This pod geometry is shown in Fig 5(b). For the fully enclosed tube simulations, the domain was taken as half of the tube with a vertical symmetry plane applied. Again, the tube walls were modelled with no-shear-stress conditions.

In order to perform simulations that are representative of a Hyperloop, a second scale (termed full-scale) was also used. For the full-scale simulations, the geometries were scaled up by a factor of ≈70 to give: $d = 3$ m, $l = 8.45$ m and $l_{\text{pod}} = 20$ m. This diameter is commonly used for Hyperloop simulations [13], and it is slightly smaller than the typical size of a conventional high-speed train. For the pod geometry, the central straight section was extended such that the overall length was 20 m. This is representative of sizes used in the Hyperloop literature [24], though it has been shown that the pod length does not have a large impact on the drag it experiences [25].

The meshing strategy used in the validation case (section II) was applied to the geometry shown in Fig 5. The introduction of tube walls meant that cells were more concentrated between pod and tube wall. As with the validation case, mesh adaption to static pressure gradient was employed. A typical mesh surrounding the full pod geometry is illustrated in Fig 6.

Downloaded by Carl Gilkeson on July 30, 2024 | http://arc.aiaa.org | DOI: 10.2514/6.2024-3770

Downloaded by Carl Gilkeson on July 30, 2024 | http://arc.aiaa.org | DOI: 10.2514/6.2024-3770

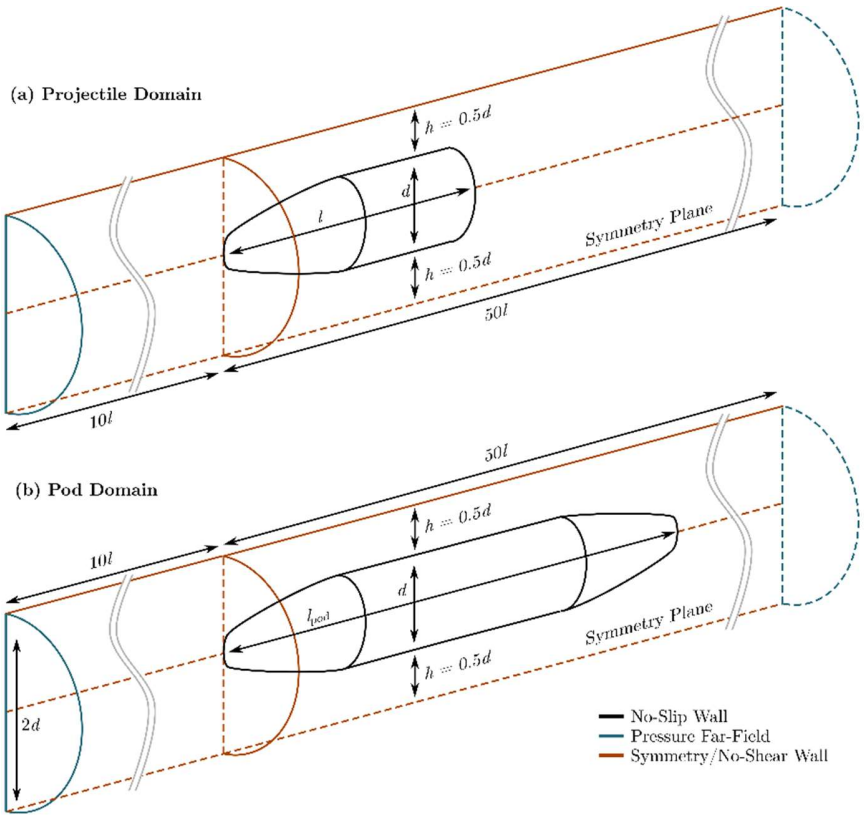

Fig. 5 Illustration of the solution domain for (a) bullet and (b) Hyperloop pod for full-scale confined flow cases.

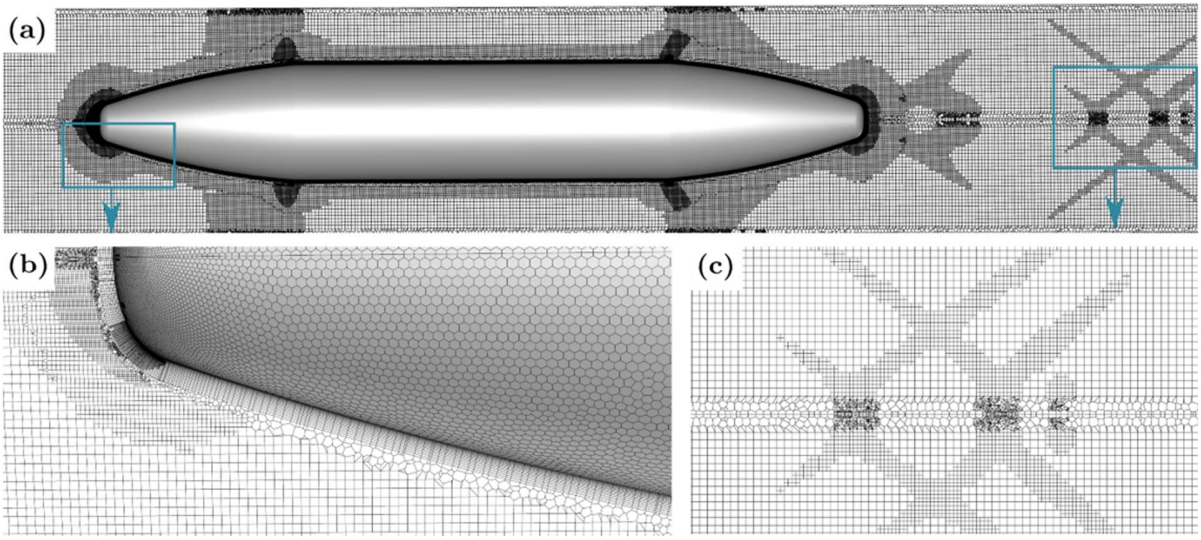

Fig. 6 Mesh structure for the confined Hyperloop case.

B. Simulation Options

In total, four different characteristics were considered to morph the validation case from section II into a realistic Hyperloop configuration, namely:

i. Scale
ii. Operating pressure
iii. Domain shape
iv. Projectile tail geometry

For each characteristic, two sub-options were considered. Firstly, in addition to the model scale from the validation case, simulations were run at an equivalent full-scale case, one large enough to fit passengers in the projectile i.e. with a vehicle diameter of 3 m. Operating pressures of atmospheric pressure and 0.1% of the atmospheric value were evaluated, to represent realistic Hyperloop operation. As well as the ground-effect configuration considered previously, full tube confinement was considered. Finally, two shapes were studied, the bullet configuration and the pod shape (recall Fig 5). For simulations involving low pressure, the Reynolds number reduced to such an extent that transition effects became important. Accordingly, these simulations utilized the transition SST turbulence model [26, 27] which has been extensively validated for such aerodynamic flows [27, 28].

C. Results Comparison

Table 3 details four key results for various combinations. The drag force, D, represents aerodynamic resistance and this is a sensible metric for comparison. For reference, the first row of data in Table 3 is from the validation simulation from section II. Configuration B shows the impact of changing from the ground-effect scenario to a full tube, with all other options unchanged. Clearly, the effect of confinement more than doubles aerodynamic drag which is because the relatively high blockage of 25% leads to choked flow within the tube. Next, configuration C illustrates the effect of simultaneously scaling down ambient air pressure whilst increasing the domain size model to full-scale. As expected, the drag force increases but interestingly, the drag coefficient, C_D, only increases marginally from 1.44 at model-scale and ambient pressure to 1.49 at full-scale in a low-pressure environment. Next, configuration D comprises the full pod shape (Fig 5(b)) in what can be considered as a Hyperloop-type low-pressure environment. The drag force reduces by 2.3% by virtue of reduced pressure drag from the boat-tailing effect. However, the change to the rear of the vehicle does not impact the degree of flow choking which is what dominates the drag levels.

Table. 3 Results comparison for various configurations.

Configuration	Object			Domain	Reynolds	Pressure,	Drag force,
	Type	Length, l (m)	Diameter, d (m)	Shape	No.	p (atm)	D (N).
A	Bullet	0.12	0.043	Ground-effect	1.1 M	1.000	83
B	Bullet	0.12	0.043	Full-tube	1.1 M	1.000	175
C	Bullet	8.45	3.000	Full-tube	74 K	0.001	888
D	Pod	20.00	3.000	Full-tube	74 K	0.001	868

Closer inspection of the flow generated in the fully enclosed environment reveals that it differs significantly from that of the ground-effect case. This is highlighted in the Mach number contour plots, projected onto the symmetry plane, for three configurations, as shown in Fig 7. Due to the central position of the bullet in the tube, Fig 7(b), the wake does not deviate from the centerline of the tube, in contrast to the ground-effect case, Fig 7(a), where the wake angles towards the ground (recall section II.D). One similarity between the ground-effect and confined-flow cases is that expansion waves still exist at geometry transition points. For the confined-flow cases, an oblique shock is generated where the flow is turned back on itself by the wake. This shock reflects and self-interacts, forming a stationary pattern of shock diamonds behind the pod, with normal shocks (or Mach disks) forming at these interactions in the vicinity of the centerline.

As already mentioned, the most significant difference with the tube simulations is the fact that the flow has choked. Flow choking is the state in which the mass flow rate past the body is limited, which causes mass to continually accumulate upstream. This generates a normal shock ahead of the body which increases separation distance to the pod nose, with time. A second normal shock is also generated downstream of the wake reflecting shock section, as the flow re-compresses to the ambient tube conditions. Again, the distance between this shock and the pod increases with time. These two transient shocks are not displayed in the results here as they are allowed to pass out of the solution

Downloaded by Carl Gilkeson on July 30, 2024 | http://arc.aiaa.org | DOI: 10.2514/6.2024-3770

domain, thereby preserving only the locally steady flow. It can be seen that the inclusion of the tapered tail on the pod-type geometry narrows the wake significantly, in comparison to the flat base geometry of the projectile. The strength of the reflecting oblique shocks is also reduced. However, flow choking still dominates the drag prediction, irrespective of the shape of the rear of the pod. This fact is illustrated by Fig 8 which shows near-identical pressure distributions at the nose of either projectile type. Overall, the results highlight that the presence of the fully enclosed tube walls have a significant impact on the flow field when compared with the ground-effect projectile results.

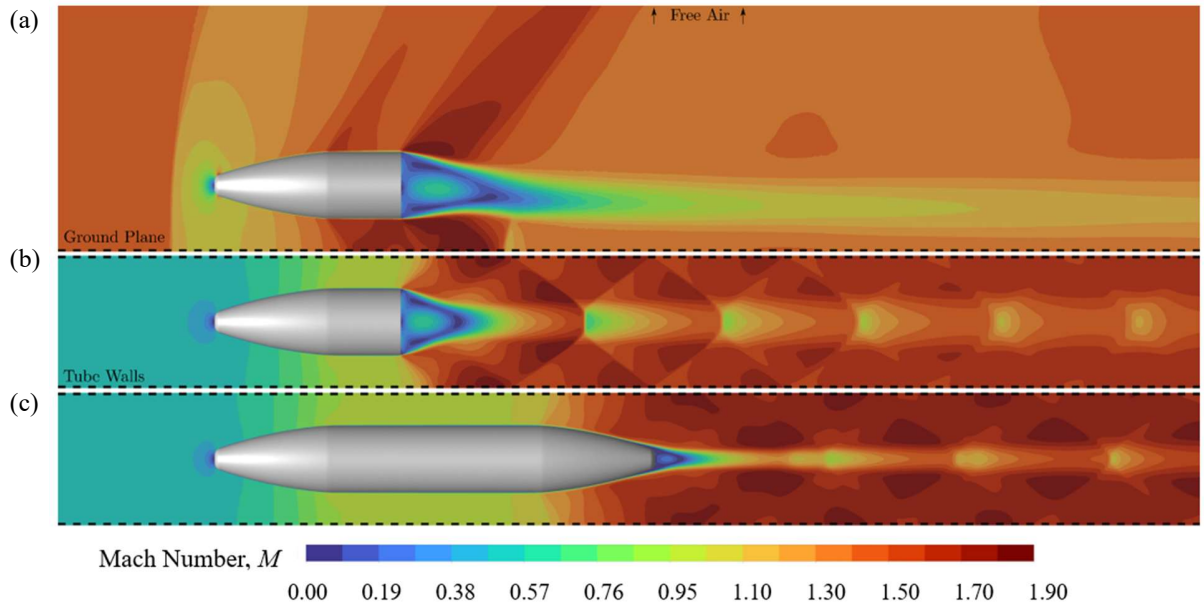

Fig. 7 Mach number contour plots project on the symmetry plane for (a) model-scale validation case [Configuration A], (b) full-scale bullet-in-tube [Configuration C], and (c) full-scale pod-in-tube cases [Configuration D].

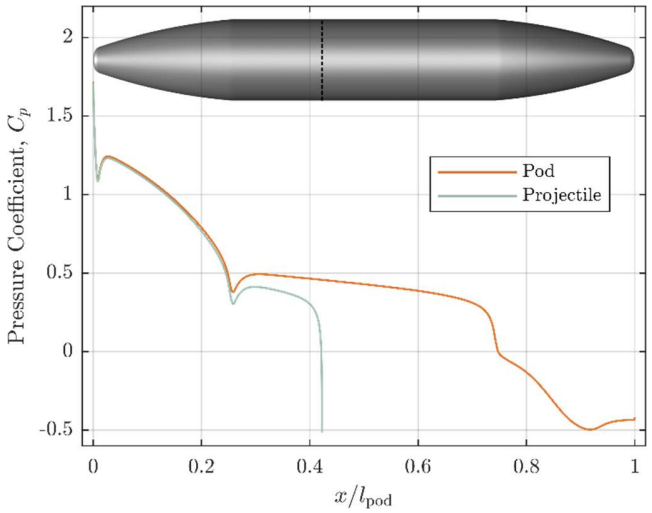

Fig. 8 Pressure coefficient distribution for confined flow results.

Downloaded by Carl Gilkeson on July 30, 2024 | http://arc.aiaa.org | DOI: 10.2514/6.2024-3770

IV. Discussion

In this article, a CFD simulation approach was proposed in an effort to predict the characteristics of a Hyperloop system. This approach was initially validated based on experimental pressure distributions, obtained on a scaled-up bullet. The results showed very good agreement between the CFD predictions and real-world measurements. Furthermore, key qualitative flow features were accurately reproduced.

A series of further simulations then considered the impact of projectile scale, operating pressure, domain shape and vehicle tail configuration. These aspects were investigated in an effort to extend the validated CFD approach to a more realistic full-scale, low-pressure and confined environment; this is the environment within which a Hyperloop vehicle is expected to operate. As previously described, the drag characteristics of a Hyperloop system are dominated by choked flow which is expected, given the necessary blockage of what is essentially a form of rail travel. Despite the unavoidable flow choking, the drag level experienced by a pod shape within a Hyperloop-type environment is just 0.3% of the equivalent full-scale, free-air value, at atmospheric pressure. This underlines the potential of the proposed pod shape and the overall concept itself.

As described in section I, a tremendous volume of research has been dedicated to the advancement of Hyperloop since the publication of Musk's high-level document in 2013 [1]. Despite a number of interesting developments, a key gap in knowledge is an experimental understanding of confined transonic flow in very-low-pressure environments. The work by [18] is an early marker for what can be expected, experimentally, but there is a long way to go. It must be emphasized here just how difficult it is to obtain physical aerodynamic measurements in Hyperloop systems.

Observing the wider literature, one aspect which is particularly striking is the complete lack of consensus for what a Hyperloop vehicle may look like. Therefore, in this article, we proposed an initial shape which is relatively simple, yet based on a real-life bullet which is specifically designed to operate in the high transonic speed regime. The encouraging results indicate that this is a suitable starting point for Hyperloop vehicle development. It is envisaged that this shape will be tested experimentally and with this, a challenge is laid out to the wider research community.

In the shorter term, the work detailed in this article is being developed with the aim of proposing benchmark cases for evaluating the accuracy of Hyperloop aerodynamics simulations. One aspect which requires particular attention is the assessment of different ground clearances instead of the central pod position within the tube cross section considered in the present study.

V. Conclusion

This paper begins to address a key problem in the advancement of Hyperloop aerodynamics, namely, the lack of a suitable benchmark case for evaluating the accuracy of numerical simulations. Here, a validated CFD simulation approach demonstrated very good agreement with pre-existing experimental measurements of flow around a bullet. This projectile shape was then used as a basis for a new Hyperloop pod shape and the results underlined the clear potential when applied to the unique demands of Hyperloop. The proposed Hyperloop system, including a suitable tube shape, offers a starting point for future research which will form a new benchmark for simulating Hyperloop aerodynamics.

Acknowledgments

This work was supported by the UK Engineering and Physical Sciences Research Council (EPSRC) grant EP/S022732/1 for the University of Leeds Centre for Doctoral Training in Fluid Dynamics. This work was undertaken on ARC3/4, part of the High Performance Computing facilities at the University of Leeds, UK. The authors thank Graham Doig and Harald Kleine for providing details of their experiments to aid the setup of the numerical validation.

References

[1] Musk, E., *Hyperloop alpha*. Tesla, SpaceX, 2013, URL https://tesla.com/sites/default/files/blog_images/hyperloop-alpha.pdf. [retrieved 20 June 2024].

[2] Prosser, R.B. Medhurst, George (1759–1827). In: *Oxford dictionary of national biography*, Oxford University Press, Oxford, England, UK, 2004.

[3] Hardenberg, H. O., *The middle ages of the internal-combustion engine, 1794-1886*, Society of Automotive Engineers, Warrendale, PA, 1999.

[4] Buchanan, R. A., "The atmospheric railway of I. K. Brunel," *Social Studies of Science*, Vol. 22, No. 2, 1992, pp. 231–243.

[5] Goddard, R. H., "The limit of rapid transit," *Scientific American*, Vol. 101, No. 21, 1909, pp. 366.

[6] Forgacs, R. L., "Evacuated tube vehicles versus jet aircraft for high-speed transportation,". *Proceedings of the IEEE*, Vol. 61, No. 5, 1973, pp. 604–616.

Downloaded by Carl Gilkeson on July 30, 2024 | http://arc.aiaa.org | DOI: 10.2514/6.2024-3770

[7] Macola, I. G., *Timeline: tracing the evolution of hyperloop rail technology*. 2021, URL https://railway-technology.com/features/timeline-tracing-evolution-hyperloop-rail-technology/. [retrieved 20 June 2024].
[8] Jufer, M., Perret, F-L., Descoeudres, F., and Trottet, Y. "Swissmetro, an efficient intercity subway system," *Structural Engineering International*, Vol. 3, No. 3, 1993, pp. 184–189.
[9] Rudolf, A. "Simulation of compressible flow in tunnel systems induced by trains traveling at high speed," Ph.D. Dissertation, EPFL Thesis No. 1806, École polytechnique fédérale de Lausanne., Lausanne, Swittzerland, 1998.
[10] Cassat, A., "Swissmetro – project development status," *Proceedings of international symposium on speed-up service technology for railway and maglev systems*, STECH'03, JSME, Tokyo, 19-22 August, 2003, pp. 453–60.
[11] SwissMetro-NG, SwissMetro-NG home page. 2024, URL https://swissmetro-ng.org/. [retrieved 20 June 2024].
[12] Lang, A. J., Connolly, D. P., de Boer, G., Shahpar, S., Hinchliffe, B., and Gilkeson, C. A., "A review of hyperloop aerodynamics," *Computers and Fluids*, Vol. 273, Article No. 106202, 2024, pp. 1–23.
[13] Jang, K. S., Le, T. T. G., Kim, J., Lee, K. S., and Ryu, J., "Effects of compressible flow phenomena on aerodynamic characteristics in Hyperloop system," *Aerospace Science and Technology*, Vol. 117, Article No. 106970, 2021.
[14] Bi, H., Wang, Z., Wang, H., and Zhou, Y., "Aerodynamic phenomena and drag of a maglev train running dynamically in a vacuum tube," *Physics of Fluids*, Vol. 34, Article No. 096111, 2022.
[15] Niu, J., Sui, Y., Yu, Q., Cao, X., Yuan, Y., and Yang, X., "Effect of acceleration and deceleration of a capsule train running at transonic speed on the flow and heat transfer in the tube," *Aerospace Science and Technology*, Vol. 105, Article No. 105977, 2020.
[16] Yu, Q., Yang, X., Niu, J., Sui, Y., Du, Y., and Yuan, Y., "Aerodynamic thermal environment around transonic tube train in choked/unchoked flow," *International Journal of Heat and Fluid Flow*, 92, Article No. 108890, 2021.
[17] Sui, Y., Yu, Q., Niu, J., Cao, X., Yang, X., and Yuan, Y., "Flow Characteristics and Aerodynamic Heating of Tube Trains in Choked/Unchoked Flow: A Numerical Study," *Journal of Thermal Science*, Vol. 32, No. 4, 2023, pp. 1421–1434.
[18] Seo, Y., Cho, M., Kim, D. H., Lee, T., Ryu, J., and Lee, C., "Experimental Analysis of Aerodynamic Characteristics in the Hyperloop System," *Aerospace Science and Technology*, Vol. 137, Article No. 108265, 2023.
[19] Doig, G., Barber, T. J., Leonardi, E., Neely, A. J., Kleine, H., and Coton, F., "Aerodynamics of a Supersonic Projectile in Proximity to a Solid Surface," *AIAA Journal*, Vol. 48, No. 12, 2010, pp. 2916–2930.
[20] Doig, G., Wang, S., Kleine, H., and Young, J., "Aerodynamic Analysis of Projectiles in Ground Effect at Near-Sonic Mach Numbers," *AIAA Journal*, Vol. 54, No. 1, 2016, pp. 150–160.
[21] ANSYS, Commercial CFD Software Package, Ver. 2020R2, Ansys, Inc., Canonsburg, PA, 2024.
[22] Menter, F. R., "Two-equation eddy-viscosity turbulence models for engineering applications," *AIAA Journal*, Vol. 32, No. 8, 1994, pp. 1598–1605.
[23] Young, J., Carriage, K., Oakes, B., Kleine, H., Hiraki, K., and Inatani, Y., "Numerical Simulation and Experiments on the Ground Effect of Transonic Projectiles," *29th International Symposium on Shock Waves*, Madison, WI, 14-19 July, 2013, In: "29th International Symposium on Shock Waves", Volume 2, Springer International, 2015, pp. 1297–1302.
[24] Niu, J., Sui, Y., Yu, Q., Cao, X., and Yuan, Y., "Numerical study on the impact of Mach number on the coupling effect of aerodynamic heating and aerodynamic pressure caused by a tube train," *Journal of Wind Engineering and Industrial Aerodynamics*, Vol. 190, 2019, pp. 100–111.
[25] Oh, J. S., Kang, T., Ham, S., Lee, K. S., Jang, Y. J., Ryou, H. S., and Ryu, J., "Numerical analysis of aerodynamic characteristics of Hyperloop system," *Energies*, Vol. 12, No. 3, 2019, p. 518.
[26] Menter, F. R., Likki, S. R., Suzen, Y. B., Huang, P. G., and Volker, S., "A Correlation-Based Transition Model Using Local Variables—Part I: Model Formulation," *Journal of Turbomachinery*, 128, 2006, pp. 413–422.
[27] Langtry, R. B., Menter, F. R., Likki, S. R., Likki, S. R., Suzen,, Huang, P. G., and Volker, S., "A Correlation-Based Transition Model Using Local Variables—Part II: Test Cases and Industrial Applications," *Journal of Turbomachinery*, 128, 2006, pp. 423–434.
[28] Langtry, R. B., and Menter, F. R., "Transition modeling for general CFD applications in aeronautics," in *43rd AIAA Aerospace Sciences Meeting and Exhibit*, Reno, NV, 10-15 January, 2013, AIAA Paper No. 2005-522.

Downloaded by Carl Gilkeson on July 30, 2024 | http://arc.aiaa.org | DOI: 10.2514/6.2024-3770